First-principles characterization of Mg low-index surfaces: Structure, reconstructions, and surface core-level shifts

Miha Gunde,[1,2] L. Martin-Samos,[1,3,*] Stefano de Gironcoli,[4] Mattia Fanetti,[1] Dmytro Orlov,[1,5] and Matjaz Valant[1,6]

[1]*Materials Research Laboratory, University of Nova Gorica, Vipavska 11c 5270-Ajdovščina, Slovenija*

[2]*Laboratory of Analysis and Architecture of Systems, Centre National de la Recherche Scientifique and University Toulouse III-Paul Sabatier, 7 avenue du Colonel Laroche, F-31400 Toulouse, France*

[3]*CNR-IOM/Democritos National Simulation Center, Istituto Officina dei Materiali, c/o SISSA, via Bonomea 265, IT-34136 Trieste, Italy*

[4]*SISSA, via Bonomea 265, IT-34136 Trieste, Italy*

[5]*Division of Materials Engineering, Department of Mechanical Engineering, Lund University, Ole Römers väg 1, Lund 22363, Sweden*

[6]*Institute of Fundamental and Frontier Sciences, University of Electronic Science and Technology of China, Chengdu 610054, China*

(Received 15 December 2017; revised manuscript received 22 May 2019; published 2 August 2019)

In this paper, first-principles calculations provide structural characterization of three low-index Mg surfaces—Mg(0001), Mg(10$\bar{1}$0), and Mg(11$\bar{2}$0)—and their respective surface core-level shifts (SCLSs). Inspired by the close similarities between Be and Mg surfaces, we also explore the reconstruction of Mg(11$\bar{2}$0). Through the calculation of surface energies and the use of the angular-component decomposed density of states, we show that reconstructions are likely to occur at the Mg(11$\bar{2}$0) surface, similarly to what was found earlier for Be(11$\bar{2}$0). Indeed, the surface energy of some of the explored reconstructions is slightly lower than that of the unreconstructed surface. In addition, because of lattice symmetry, the morphology of the unreconstructed surface (11$\bar{2}$0) results in a steplike zig-zag chain packing, with topmost chains supporting a resonant, quasi-one-dimensional (1D), partially filled electronic state. As the presence of partially filled quasi-1D bands is a necessary condition for Peierls-like dimerization, we verify that the undimerized surface chain remains stable with respect to it. Some of the reconstructions, namely, the 2×1 and 3×1 added row reconstructions, induce a stronger relaxation of the topmost chains, increasing the coupling with lower layers and thus significantly damping the quasi-1D character of this state. The original approach followed offers a common and general framework to identify quasi-1D bands—even in the case of resonant electronic surface states—and to meaningfully compare calculated and measured SCLSs even in the presence of multicomponent peak contributions.

DOI: 10.1103/PhysRevB.100.075405

I. INTRODUCTION

In the modern age of high-performance yet sustainable material design, magnesium-based metals shine in both structural and functional applications. These include light-weight structural components in vehicles and electronics, bio-resorbable implants in medicine, and hydrogen storage materials for energy [1,2], to name a few. The characteristics of magnesium enabling such applications are its low density (the lowest among structural metals) and its high chemical reactivity. The latter often also represents the main limiting factor, causing unacceptably high degradation rates [3]. Mitigating this is complicated, since degradation phenomena on magnesium surfaces are still poorly understood, especially at the atomic-scale level. The hexagonal close-packed lattice of Mg usually causes strong crystallographic texture development during fabrication, which calls for an in-depth investigation of low-index surface planes. Such deep understanding requires a detailed model of the pristine surface structure, including relaxations and reconstructions, as both will determine the physico-chemical properties of the surfaces.

Besides the aforementioned interest and related challenges in Mg applications, the fundamental study of Mg has been closely related to anomalies found in Be. Comparative studies between low-index surfaces of the two elements have found many similarities. Among others are (i) the expansion of the 0001 surface layer [4–9] (in contrast with the traditional simple theory of metals [10]), (ii) the large multilayer relaxation, and (iii) the oscillatory thermal expansion of the (10$\bar{1}$0) surface [11–14]. However, after the work of Cho *et al.* [11] in 2000, where Be(10$\bar{1}$0) only was found to exhibit surface core-level shift (SCLS) oscillations, Mg was relegated to the category of simple metals, thus reinforcing the idea that Be surface anomalies were to be ascribed to its semimetallicity. The fundamental interest in Mg surfaces was not renewed until recently, despite Ismail *et al.* [13] reporting a remarkable oscillatory surface thermal expansion in both Mg(10$\bar{1}$0) and Be(10$\bar{1}$0) in 2001.

In addition to the aforementioned peculiarities, Be is the only simple metal known to reconstruct [15–17] in standard conditions, although very recently the reconstruction of a K surface under high tensile stress [18] was reported. This peculiarity is usually attributed to the atypical bonding nature of Be [19–21] that induces a band structure with energy gaps in a large portion of the Brillouin zone near the Fermi energy, i.e., a band structure more prototypical of a semimetal.

*Corresponding author: marsamos@sissa.it

In 2016, Li *et al.* [22] challenged the idea that Dirac node lines are a peculiar feature of topological insulators, by predicting their presence at the (0001) surface of Be and other alkaline-earth metals, including Mg. This revived the discussion about the importance of atomic arrangement over bonding nature.

In the present paper, we use first-principles calculations to provide a full characterization of three low-Miller-index Mg surfaces, from structure to SCLSs, including possible reconstructions inspired by the similarities between Be and Mg surfaces. Our results predict that the Mg(11$\bar{2}$0) surface may reconstruct. Indeed, the surface energy of some of the explored reconstructions is slightly lower than the unreconstructed one. Because of the lattice symmetry, the morphology of the unreconstructed surface results in a steplike zig-zag chain packing, with the topmost chains supporting a resonant, quasi-one-dimensional (1D), partially filled electronic state. The existence of a Peierls-like dimerization is ruled out by our calculations, verifying that the undimerized surface chain remains locally stable against it. On the other hand, some of the predicted reconstructions, namely, the 2×1 and 3×1 added row (AR) reconstructions, induce a stronger relaxation of the topmost chains, increasing the coupling with the lower layers and thus destroying the quasi-1D character of the state. In addition, the approach followed provides a common and general framework to identify partially filled quasi-1D bands, even in the case of resonant surface states. We develop an original methodology to compute depth-weighted SCLSs, allowing a meaningful comparison with measured SCLSs when the surface exhibits multicomponent peak contributions, as is the case for the predicted reconstructions.

II. COMPUTATIONAL APPROACH

The calculations presented in this paper are based on density functional theory as implemented in the QUANTUM ESPRESSO distribution [23]. We adopt the Perdew-Burke-Ernzerhof (PBE) exchange-correlation functional [24] and ultrasoft pseudopotentials as provided in the PSlibrary [25] collection, namely, the Mg.pbe-nl-rrkjus.UPF dataset. Wave functions and densities are expanded in a basis of plane waves up to a kinetic-energy cutoff of 58 and 358 Ry, respectively. Slabs of 11, 20, and 15 layers are used to model the Mg(0001), Mg(10$\bar{1}$0), and Mg(11$\bar{2}$0) surfaces, respectively, resulting in similar thicknesses. For the calculation of the SCLS, a core-excited pseudopotential was generated introducing a hole in the Mg $2p$ core state, assuming the same cutoff radii, projectors, and hardness as the original Mg.pbe-nl-rrkjus.UPF. Atomic tests on the transferability and robustness of the generated pseudopotential give an all-electron vs pseudopotential error of less than 10 meV for excited atomic configurations up to 5 eV. In order to minimize interactions between periodic replicas in the final-state SCLS calculations we used 3×3, 3×2, and 4×4 surface supercells for Mg(0001), Mg(10$\bar{1}$0), and Mg(11$\bar{2}$0), respectively. With this choice, all cells have a comparable surface area of aspect ratio close to unity. Accordingly, the Brillouin zone was sampled with an equivalent Monkhorst-Pack k-point mesh of 8×8 for the periodic directions. Benchmark calculations on selected surface models have also been performed within the local-density approximation (LDA) (see Supplemental Material [26]). LDA pseudopotentials were generated with the same cutoff radii, projectors, and hardness as Mg.pbe-nl-rrkjus.UPF, and displayed equivalent transferability and robustness.

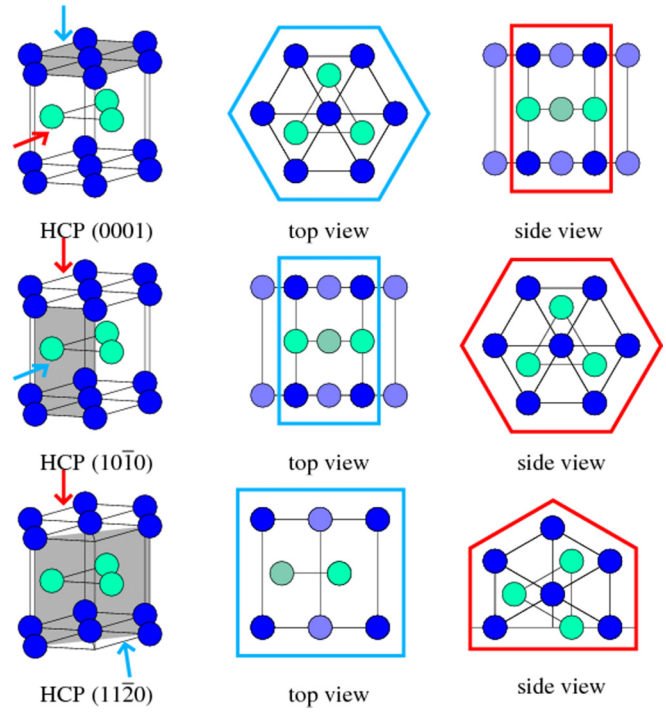

FIG. 1. Planes in the hcp crystal and side and top views of the three different Mg crystal surfaces.

III. SURFACE STRUCTURE AND SURFACE ENERGY

Magnesium crystallizes in the hexagonal close-packed (hcp) structure with lattice parameters $a = 320.9$ pm, $c = 521.0$ pm, and $c/a = 1.62$ [27]. The three surfaces under investigation, Mg(0001), Mg(10$\bar{1}$0), and Mg(11$\bar{2}$0), are shown in Fig. 1 (top and side views) together with the corresponding cutting plane in the unit cell of the respective hcp crystal. Table I reports the calculated values of the bulk equilibrium lattice parameters, obtained after a full relaxation using the computational approach described in the previous section.

TABLE I. Theoretical bulk equilibrium lattice parameters compared with literature values. For the cited theoretical references the exchange-correlation functional used (LDA or PBE) is specified. The experimental value [27] corresponds to the equilibrium lattice parameter of Mg measured at ambient temperature.

	a (Å)	c/a
This paper (PBE)	3.19	1.62
Ref. [28] (LDA)	3.12	1.62
Ref. [11] (LDA)	3.13	1.62
Ref. [29] (LDA)	3.11	1.62
Ref. [30] (LDA)	3.13	1.62
Ref. [30] (PBE)	3.20	1.62
Exp. [27]	3.21	1.62

TABLE II. Interlayer distances d and deviation in percent with respect to the equivalent ideal bulk distance for Mg(0001), Mg($10\bar{1}0$), and Mg($11\bar{2}0$). d_{ij} denotes the distance between the ith and jth layer. Layer 1 is the topmost layer.

	(0001)	($10\bar{1}0$)	($11\bar{2}0$)
d_{12}	2.63 (+1.2%)	0.73 (−19.2%)	1.47 (−7.2%)
d_{23}	2.60 (+0.2%)	2.01 (+8.0%)	1.65 (+4.5%)
d_{34}	2.59 (−0.1%)	0.81 (−10.7%)	1.58 (−0.4%)
d_{45}	2.59 (−0.2%)	1.94 (+4.4%)	1.59 (+0.4%)

In agreement with previous experimental and computational works [28–33], and similarly to Be(0001), the calculated distance between the topmost and second surface layer in Mg(0001) is larger than the bulk value, whereas variations of deeper interlayer distances are negligible (see Table II). The clear distinction between the topmost layer and deeper layers makes the identification of "surface atoms" and "bulk atoms" unambiguous in Mg(0001). The Mg($10\bar{1}0$) surface behaves quite differently, as can be seen from Table II. Two typical interlayer distances exist, a short one and a long one, resulting in the stacking of bilayers. Compared to bulk values, the calculated first (short) interlayer distance is shorter while the second one is longer, resulting in an overall shrinking of the bilayer together with an overall increase of the bilayer-to-bilayer distance. The most interesting difference between Mg(0001) and Mg($10\bar{1}0$) comes from the oscillations in the interlayer distances, already reported in Refs. [11,12,29,33] and confirmed here (see also Table 1 from Supplemental Material [26] for the LDA comparison). The Mg($11\bar{2}0$) surface presents one characteristic interlayer distance. Because of the lattice symmetry, the morphology of the surface results in a steplike zig-zag chain packing. The overall relaxation effect (see Table II) is a shrinking of the first interlayer separation together with an increase of the second one (see also Ref. [29]). However, contrary to Mg($10\bar{1}0$) but similarly to Mg(0001), the oscillations of the interlayer distances are negligible after the second layer.

Considering the reconstruction patterns explored by Stumpf *et al.* [21] for Be($11\bar{2}0$), we have explored 2×1 and 3×1 AR and missing row (MR) surfaces, as well as 4×1 MR reconstructions for Mg($11\bar{2}0$). All results are summarized in Table III. The unrelaxed surface morphology with an added/missing row appears as a series of Mg atomic chains along the [001] direction lying on an ideal Mg($11\bar{2}0$) substrate (see, for instance, Fig. 2, comparing the unreconstructed surface with the 3×1 AR reconstruction). The reconstructed surfaces exhibit a periodic corrugation. The symmetry reduction along the [010] direction makes the atomic relaxation along this direction slightly different depending on the lateral distance from the topmost atomic chains. This is more evident at the first layer atoms of the "substrate" and those of the second layer immediately underneath the chain. Two effects are competing: one is the expected inwards relaxation of interlayer distances for atoms that have a reduced number of neighbors along the direction perpendicular to the surface; the second is related to Friedel oscillations that induce inward or outward relaxations. In general, the oscillatory behavior of interlayer distances is more pronounced than in the unreconstructed case. Interestingly, in the 2×1 and 3×1 AR structures the additional chain sits at an interlayer distance significantly shorter than in the unreconstructed case or in the other explored reconstructions. As a consequence, the coupling between the topmost chain and the underlying layers is expected to be stronger for the 2×1 and 3×1 AR reconstructions than for all other surface morphologies, and this has consequences for the surface electronic structure (see later).

TABLE III. Interlayer distances d and deviation in percent with respect to the equivalent ideal bulk distance for Mg(0001), Mg($10\bar{1}0$), and Mg($11\bar{2}0$) [the deviation with respect to bulk distances is calculated with full accuracy (double precision); variations between the reported percentage and distances are due to rounding errors]. d_{ij} denotes the distance between the ith and jth layer. The topmost chain(s) has index 1. The atomic configuration for 2×1 symmetry is identical for MR or AR.

	2×1	3×1 AR	3×1 MR	4×1 MR
d_{12}	1.39 (−11.9%)	1.39 (−11.9%)	1.45 (−8.5%)	1.47 (−7.2%)
d_{23}	1.70 (+7.7%)	1.70 (+7.7%)	1.65 (+3.8%)	1.65 (+3.8%)
d_{34}	1.53 (−2.9%)	1.53 (−2.9%)	1.58 (−0.2%)	1.58 (−0.1%)
d_{45}	1.60 (+1.0%)	1.61 (+1.0%)	1.57 (−1.1%)	1.59 (−0.01%)

Our calculated surface energies are reported in Table IV, together with some results from literature. In Ref. [29] the surface energy of Mg(0001) was found to be significantly lower than for the other two surfaces (see also Refs. [28,31,32,34] for other LDA values), and our calculations confirm this trend. The authors of Ref. [29] speculated about the possible stabilization of Mg($10\bar{1}0$) and Mg($11\bar{2}0$) surfaces through reconstruction and/or defect formation driven by surface stress. Indeed, according to Payne *et al.* [35], both surfaces exhibit a value for one of the surface-stress components (multiplied by the surface area per atom) larger than the bulk cohesive energy, satisfying a proposed criterion for structural instability. However, as reconstruction was not observed in Mg($10\bar{1}0$) [11], the authors concluded, for both ($10\bar{1}0$) and ($11\bar{2}0$) surfaces, that the stabilization should arise from the presence of defects. From our calculations, however, the presence of reconstructions at Mg($11\bar{2}0$) cannot be ruled out as some of the reconstructed surfaces exhibit a surface energy slightly lower than the unreconstructed surface, with quasidegenerate values. This result is robust with respect to the choice of the exchange and correlation functional (see Table 3 from Supplemental Material [26] for the LDA results). Surfaces with a high concentration of isolated adatoms/vacancies have clearly higher surface energies. The behavior of Mg($11\bar{2}0$) surfaces with respect to reconstructions is very similar to what was found for the Be($11\bar{2}0$) surface [15,16] which is known to display a 3×1 reconstruction.

IV. ELECTRONIC STRUCTURE

The origin of the reconstruction in the ($11\bar{2}0$) surface can be traced back to the high surface energy of the unreconstructed surface. On the sole basis of the surface energy, we can predict that 2×1 and/or 3×1 AR reconstructions may

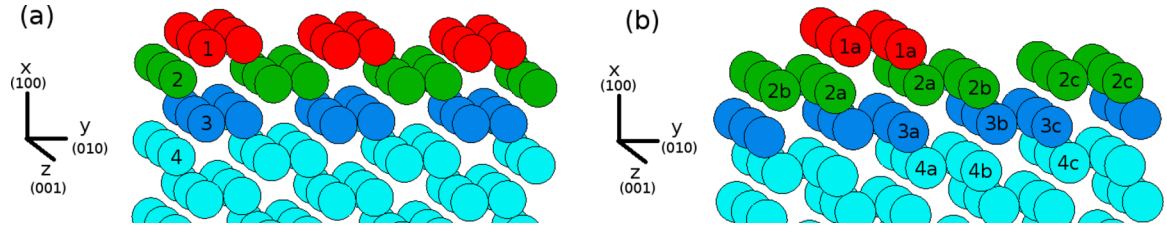

FIG. 2. Structure of the unreconstructed (a) and 3 × 1 AR reconstructed (b) Mg(11$\bar{2}$0) surface. Topmost Mg chains are highlighted in red.

occur. A closer analysis of the surfaces electronic structure and, in particular, of the atom-projected orbital-decomposed density of states (p-DOS) provides some additional arguments in favor of the aforementioned reconstructions. The total DOS of the three surface slabs exhibits the expected $\sqrt{E}$ behavior typical of a three-dimensional (3D) nearly free electron metal. The surface-atom p-DOS would be expected to exhibit a similar behavior, possibly turning toward a flat dependence typical of two-dimensional nearly free electrons. Indeed, this is what we observe for all three surfaces, for the angular-projected components s, $2p_z$, and $2p_y$ that are coplanar with the surface planes. Surprisingly, only the $2p_y$-projected p-DOS [see Fig. 3(a)] of the unreconstructed Mg(11$\bar{2}$0) surface strongly deviates from a $\sqrt{E}$ or constant behavior with a series of peaks around 1 eV below (and slightly above) the Fermi energy. These peaks are reminiscent of the energy levels of free electrons confined in a finite cylindrical potential well (see Ref. [36]), with energy values depending on a principal quantum number, $n = 1, 2, \ldots$, and an angular (cylindrical) quantum number, $m = 0, 1, 2, \ldots$. In the limit of an infinitely deep potential well, these tend to the nth zeros ($z_m^{(n)}$) of the J_m Bessel function. The finite depth of the well shrinks the peaks to lower energies (see dot-dashed vertical red lines in Fig. 3). Identical features have been observed in nanowires (see Fig. 3 of Ref. [37]). Top layer Mg atoms in the ideally terminated Mg(11$\bar{2}$0) surface form zig-zag chains along the [001] crystallographic direction, which support a partially filled, quasi-1D, surface-localized band originating from the overlap of Mg $2p_x$ orbitals. The resonant character of this band makes it difficult to precisely quantify its dispersive character in the k-resolved surface band structures (k-resolved p-DOS), while its signature is easily observed in the angular-component decomposed pDOSs (see Fig. 3).

As the presence of a partially filled quasi-1D band is a necessary condition for the existence of a Peierls-type dimerization, we performed calculations doubling the cell dimension along the zig-zag chains (along z) and forcing a starting configuration with Mg-Mg bond alternation. Surprisingly, the dimerized surface was found to be unstable, and to relax back to the ideal undimerized case. Therefore, our calculations rule out the Peierls mechanism as possible driving force for the reconstruction.

Among the investigated reconstructions, the peak structure in the p-DOS disappears for the 2 × 1 and 3 × 1 AR reconstructions, while the peaks are still present in the orbital-resolved $2p_y$ component of the 3 × 1 and 4 × 1 MR reconstructions. As previously mentioned, the inward relaxation of the topmost chains in the 2 × 1 and 3 × 1 AR is significantly larger than that in the other explored reconstructions (see Table III). This strengthens the coupling between the chain and the "substrate" layers, thus reducing the quasi-1D

TABLE IV. Calculated surface energy (meV/Å^2) for the three unreconstructed surfaces (001, 100, and 110) and for the MR or AR reconstructions with different symmetry on Mg(11$\bar{2}$0). The atomic configuration for 2 × 1 symmetry is identical for MR or AR. To compare with previous ideas [29] that the Mg(11$\bar{2}$0) might be stabilized by the presence of point defects, the 3 × 1 and 4 × 1 missing atom (MA) and 2 × 1 and 3 × 1 added atom (AA) surface energies are also reported. "t.w." is used to indicate the results obtained in this paper.

	(0001)	(10$\bar{1}$0)	(11$\bar{2}$0)
t.w.	30	38	45
Ref. [29]	40	44	53
Ref. [30]	35		
	Reconstructed (11$\bar{2}$0)		
2 × 1	3 × 1 AR	3 × 1 MR	4 × 1 MR
44	44	45	47
	Added/missing atom at (11$\bar{2}$0)		
3 × 1 MA	4 × 1 MA	2 × 1 AA	3 × 1 AA
48	47	49	48

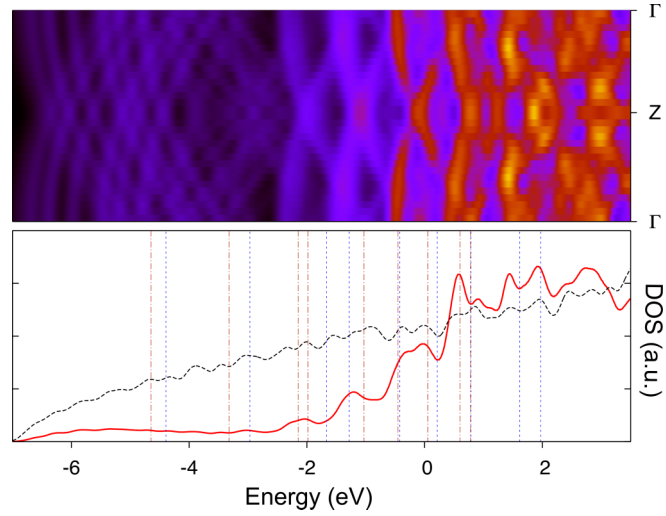

FIG. 3. Total p-DOS (black dashed line), p_y projection at the first layer atom of the unreconstructed Mg(11$\bar{2}$0) surface (red continuous line), and k-resolved p_y density of states. Vertical dashed lines indicate the first nine quantized energy levels for 3D electrons in a cylindrical potential well with finite (red dot-dashed lines) and infinite (blue dashed lines) depth. For the finite depth case, a $\nu = 10$ value has been used [see Eq. (3) of Ref. [36]).

TABLE V. Individual-layer calculated SCLSs (meV) for Mg(0001), Mg($10\bar{1}0$), and unreconstructed Mg($11\bar{2}0$). The numerical error is estimated to be of the order of 10 meV and accounts for the overall convergence parameters and the robustness of the *ad hoc* generated core-hole pseudopotential. *ij* denotes the *i*th and *j*th layer with 1 being the topmost layer. XPS Δ_{B-S} is an experimentally determined SCLS, with Δ_{B-S} being the energy difference at peak maximum between the fitted bulk (B) and surface (S) component.

Layers	(0001)	($10\bar{1}0$)	($11\bar{2}0$)
12	+130	+110	+170
23	+0	+50	+10
34	−10	−20	−0
45	−10	+50	+10
XPS Δ_{B-S}[39]	140		

character of the electronic structure associated to the chain, and consequently reducing the high surface metallicity originated from the quasi-1D state.

Considering both the predicted slightly favorable surface energies and the increased coupling of the surface chain with the substrate, we predict that the most probable candidates for the reconstruction of Mg($11\bar{2}0$) are the 2×1 and/or 3×1 AR. This is similar to the case of Be($11\bar{2}0$), that has been reported to reconstruct with a 3×1 symmetry [15], most probably by the AR mechanism [21].

V. SURFACE CORE-LEVEL SHIFTS

Core-level spectroscopy is an element-specific, environment-sensitive probe of a material. As such, it has been extensively employed in surface science investigations [16,38] and used to address even subtle structural properties when sufficient resolution can be attained [13]. We report here our theoretically predicted surface core-level shifts for the Mg surfaces investigated, comparing with the few available experimental results. First of all, in agreement with previous works on Mg(0001) [33,39] and Mg($10\bar{1}0$) [12], the calculated SCLSs for the top to second layer in all three unreconstructed surfaces are positive and well separated from the other shifts (see Table V). Calculated SCLSs for the Mg(0001) are in very good agreement with the measured value of 140 meV in Ref. [39] and converge very fast to the bulk value. To the best of our knowledge, experimental values for surface core-level shifts for the other two surfaces have not been reported in the literature yet.

It is worth noting that, contrary to what is reported in Ref. [12], our calculations display SCLS oscillations for the Mg($10\bar{1}0$) surface, similar to those for the Be($10\bar{1}0$) surface, regardless of the flavor of the exchange-correlation functional used (see Table 2 from Supplemental Material [26] for LDA results). As a consequence of the distinct multicomponent contributions of the SCLS in Mg($10\bar{1}0$), reported in Table V, the assignment of the position of the bulk peak in experimental x-ray photoemission spectroscopy (XPS) spectra might not be straightforward, especially if the experimental resolution is limited. As such, a meaningful comparison between theoretical and experimental SCLSs will depend on the penetration depth of the XPS probe and the overall resolution of the experimental setup.

TABLE VI. Individual-layer calculated SCLSs (meV) for reconstructed 2×1 and 3×1 AR Mg($11\bar{2}0$) taking as reference the total energy of a deep Mg atom with a hole in the core. The numerical error is estimated to be of the order of 10 meV and accounts for the overall convergence parameters and the robustness of the *ad hoc* generated core-hole pseudopotential. *i* denotes the *i*th layer along the (100) direction and *a*, *b*, and *c* refer to site positions along (010), with 1*a* being the atoms from the topmost layer (the topmost chain, see Fig. 2). Because of symmetry *c* sites are equivalent to *b* sites in 2×1.

	2×1		
Layers	*a*	*b*	*c*
1	+130		
2	+38	+147	
3	−17	+2	
4	−18	+0	
	3×1 AR		
1	+150		
2	+60	+160	+190
3	+10	+10	+50
4	+10	+10	+20

In the case of the unreconstructed ($11\bar{2}0$), similarly to the (0001) surface, a well-defined surface peak is predicted with a quite large shift of 170 meV with respect to the second layer and very little depth dependence.

In the case of the predicted AR reconstructed ($11\bar{2}0$) surface models, the situation is more complex, since a number of different values for the SCLS are computed in the first few layers as a function of the relative position of the near-surface atom with respect to the added row. In Table VI the calculated core-level shifts of near-surface atoms with respect to a bulk reference atom, located close to the center of the surface slab, are collected [see Fig. 2(b) for the labelling of the different surface atoms]. Two broad regions can be distinguished: on one end a number of contributions are below 50–60 meV from the reference bulk atoms; unless very high resolution spectra can be acquired, these are likely to contribute to the bulk peak, with different weights depending on the penetration depth of the impinging light and escape length of the outgoing electrons. On the other end contributions in the 130–190-meV range will determine a multicomponent "surface" peak. Similarly to the Mg($10\bar{1}0$) surface, the value of the $S - B$ core-level shift to be observed in an XPS experiment on Mg($11\bar{2}0$) is difficult to predict as it will critically depend on the penetration depth and the experimental resolution. We can, however, give a rough estimate of this difference that might help to discriminate between reconstructed and unreconstructed surfaces. We first impose a Gaussian broadening to each individual-layer SCLS; we then choose a penetration depth value between 3 and 5 Å: each Gaussian is multiplied by an exponential decay, e^{-d_{1n}/δ_p}, with d_{1n} being the distance between the *n*th layer and the topmost layer and δ_p being the penetration depth. The Gaussian returns the value of 1 when the topmost layer contributes with a single-component SCLS.

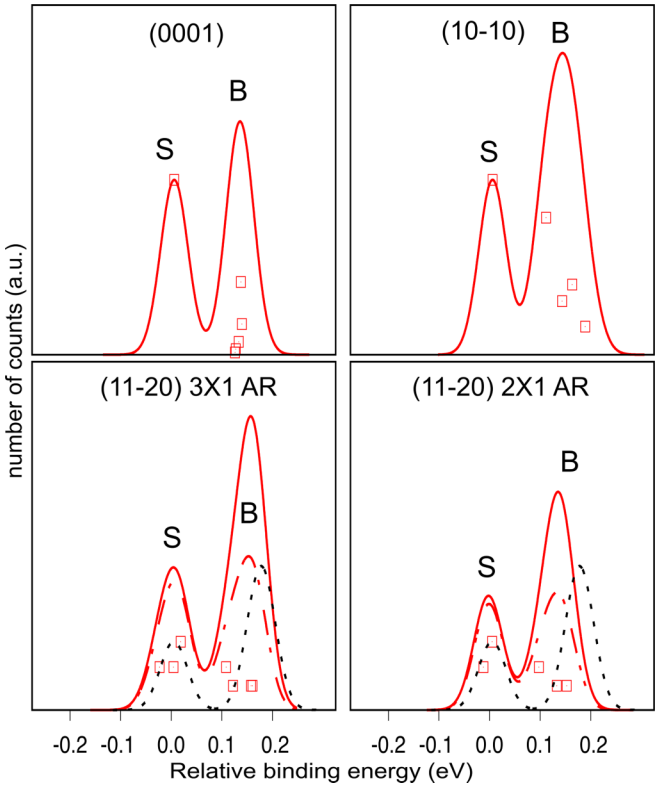

FIG. 4. Depth-weighted SCLSs for Mg(0001) and Mg(10$\bar{1}$0) and for 2×1 and 3×1 AR reconstructions at Mg(11-20) (red solid lines), and for the unreconstructed Mg(11$\bar{2}$0) (black dotted lines), for a penetration depth of 5 Å. For the reconstructed surfaces, depth-weighted SCLSs at a penetration depth of 3 Å are also shown (red dash-dotted lines). The energies have been aligned to the surface peak maxima (S) of the (0001) surface. Red squares mark the position of individual layer SCLSs. Their respective height corresponds to the intensity of the exponential decay, e^{-d_{1n}/δ_p}, with d_{1n} being the distance between the nth layer and the topmost layer, and δ_p being the penetration depth. The Gaussians have a broadening of 50 meV.

We then calculate the core-level energy difference between S and B peaks (Δ_{S-B}) from the difference between peak maxima (see Fig. 4). Δ_{S-B} are dependent on the penetration depth only in the case of multicomponent contributions. Calculated Δ_{S-B} for the unreconstructed surfaces are 130, 120, and 170 meV for Mg(0001), Mg(10$\bar{1}$0), and Mg(11$\bar{2}$0), respectively. The calculated Δ_{S-B} for the 2×1 and 3×1 AR reconstructions are between 120–130 and 140–150 meV, depending on the chosen penetration depth. In spite of the uncertainty originating from the penetration depth definition, the difference between the resulting Δ_{S-B} for the reconstructed and the unreconstructed surface is significant; no less than 20–30 meV. Moreover, as the surface peak of the reconstructed (11$\bar{2}$0) is multicomponent, contrary to the corresponding peak of (0001) and (10$\bar{1}$0) surfaces, it exhibits an intrinsic broadening. In a high-resolution XPS experiment it would be possible to determine whether the Mg(11$\bar{2}$0) surface is reconstructed or not from the position and the apparent broadening of the surface peak.

VI. CONCLUSIONS

We have studied by first-principles calculations the structural and the SCLS properties of three low-index surfaces of magnesium. We found SCLS oscillations at the Mg(10$\bar{1}$0) surface analogous to the ones previously reported for Be(10$\bar{1}$0) and more favorable surface energies for reconstructed Mg(11$\bar{2}$0) surfaces, again similar to the behavior previously reported for belyllium. Moreover, from p-DOS, we found that the unreconstructed Mg(11$\bar{2}$0) surface is electronically unstable. The use of p-DOSes provides a simple indicator of the quasi-1D character of the surface state even when the involved band is only a resonance. This kind of representation can, therefore, be used to theoretically predict the existence of such instabilities that may drive to reconstructions and/or charge density wave phases. Due to their lower surface energy and the lifting of the electronic instability, the 2×1 and the 3×1 AR reconstructions (or a mixture of the two) are good candidates for Mg(11$\bar{2}$0) surface morphology, similarly to Be(11$\bar{2}$0) that reconstructs with a 3×1 periodicity. Our results show the strong similarities between Be and Mg surfaces and highlight the role of the lattice and the underlying atomic arrangements over peculiar bonding features.

ACKNOWLEDGMENTS

We are grateful to Prof. Paolo Giannozzi, Prof. Alice Ruini, and Dr. Luigi Giacomazzi for useful discussions. We also acknowledge Prof. Erio Tosatti for his advice during the preparation of the paper. The computer time was mainly provided by CINECA through the IsC44 HP10CQGOFM project. This work has received funding from the EU-H2020 research and innovation programme under Grant No. 654360, having benefited from the access provided by CNR-IOM in Trieste (Italy) within the framework of the NFFA–Europe Transnational Access Activity, and under Grant No. 676531 (E-CAM project). Support by the Slovenian Research Agency (Research Core Funding No. P2-0377 and Project Funding No. J2-7157) and Biomag project is also acknowledged.

[1] *Magnesium Technology 2018*, edited by K. N. S. Dmytro Orlov, Vineet V. Joshi, and N. R. Neelameggham (Springer, New York, 2018).
[2] T. M. Pollock, Science **328**, 986 (2010).
[3] M. Esmaily, J. E. Svensson, S. Fajardo, N. Birbilis, G. S. Frankel, S. Virtanen, R. Arrabal, S. Thomas, and L. G. Johansson, Prog. Mater. Sci. **89**, 92 (2017).
[4] H. Davis, J. Hannon, K. Ray, and E. Plummer, Phys. Rev. Lett. **68**, 2632 (1992).
[5] P. Sprunger, L. Petersen, E. Plummer, E. Laegsgaard, and F. Besenbacher, Science **275**, 1764 (1997).
[6] K. Pohl, J. Cho, K. Terakura, M. Scheffler, and E. Plummer, Phys. Rev. Lett. **80**, 2853 (1998).
[7] M. Lazzeri and S. de Gironcoli, Phys. Rev. Lett. **81**, 2096 (1998).
[8] I. Vobornik, J. Fujii, M. Hochstrasser, D. Krizmancic, C. E. Viol, G. Panaccione, S. Fabris, S. Baroni, and G. Rossi, Phys. Rev. Lett. **99**, 166403 (2007).

[9] See J. C. Boettger and S. B. Trickey, Phys. Rev. B **32**, 1356 (1985), wherein the authors predicted a large expansion of a beryllium dilayer.

[10] J. Inglesfield, Rep. Prog. Phys. **45**, 223 (1982).

[11] J.-H. Cho, Ismail, Z. Zhang, and E. W. Plummer, Phys. Rev. B **59**, 1677 (1999).

[12] J.-H. Cho, K. S. Kim, S.-H. Lee, M.-H. Kang, and Z. Zhang, Phys. Rev. B **61**, 9975 (2000).

[13] Ismail, E. W. Plummer, M. Lazzeri, and S. de Gironcoli, Phys. Rev. B **63**, 233401 (2001).

[14] M. Lazzeri and S. de Gironcoli, Phys. Rev. B **65**, 245402 (2002).

[15] J. Hannon, E. Plummer, R. Wentzcovitch, and P. Lam, Surf. Sci. **269–270**, 7 (1992).

[16] L. Johansson, H. Johansson, E. Lundgren, J. Andersen, and R. Nyholm, Surf. Sci. **321**, L219 (1994).

[17] See R. Ludeke and G. Landgren, Phys. Rev. Lett. **47**, 875 (1981); there is a controversy on a reported Al reconstruction, which was never confirmed either experimentally or by independent theoretical calculations; see also footnote number 49 in Ref. [21]

[18] F. Yin, S. Kulju, P. Koskinen, J. Akola, and R. E. Palmer, Sci. Rep. **5**, 10065 (2015).

[19] T. Loucks and P. Cutler, Phys. Rev. **133**, A819 (1964).

[20] M. Y. Chou, P. K. Lam, and M. L. Cohen, Phys. Rev. B **28**, 4179 (1983).

[21] R. Stumpf, J. B. Hannon, P. J. Feibelman, and W. E. Plummer, The unusual properties of the beryllium surface, Report No. SAND–94-3025C (2005), https://inis.iaea.org/search/search.aspx?orig_q=RN:26044157.

[22] R. Li, H. Ma, X. Cheng, S. Wang, D. Li, Z. Zhang, Y. Li, and X.-Q. Chen, Phys. Rev. Lett. **117**, 096401 (2016).

[23] P. Giannozzi, S. Baroni, N. Bonini, M. Calandra, R. Car, C. Cavazzoni, D. Ceresoli, G. L. Chiarotti, M. Cococcioni, I. Dabo, A. Dal Corso, S. de Gironcoli, S. Fabris, G. Fratesi, R. Gebauer, U. Gerstmann, C. Gougoussis, A. Kokalj, M. Lazzeri, L. Martin-Samos, N. Marzari, F. Mauri, R. Mazzarello, S. Paolini, A. Pasquarello, L. Paulatto, C. Sbraccia, S. Scandolo, G. Sclauzero, A. P. Seitsonen, A. Smogunov, P. Umari, and R. M. Wentzcovitch, J. Phys.: Condens. Matter **21** 395502 (2009).

[24] J. Perdew, K. Burke, and M. Ernzerhof, Phys. Rev. Lett. **77**, 3865 (1996).

[25] A. Dal Corso, Comput. Mater. Sci. **95**, 337 (2014).

[26] See Supplemental Material at http://link.aps.org/supplemental/10.1103/PhysRevB.100.075405 for LDA-GGA selected comparisons.

[27] C. Kittel, *Introduction to Solid State Physics* (Wiley, New York, 2004).

[28] A. Wright, P. Feibelman, and S. Atlas, Surf. Sci. **302**, 215 (1994).

[29] P. Staikov and T. S. Rahman, Phys. Rev. B **60**, 15613 (1999).

[30] J. Da Silva, C. Stampfl, and M. Scheffler, Surf. Sci. **600**, 703 (2006).

[31] P. Sprunger, K. Pohl, H. Davis, and E. Plummer, Surf. Sci. **297**, L48 (1993).

[32] Ismail, Ph. Hofmann, A. P. Baddorf, and E. W. Plummer, Phys. Rev. B **66**, 245414 (2002).

[33] J.-J. Tang, X.-B. Yang, L. OuYang, M. Zhu, and Y.-J. Zhao, J. Phys. D: Appl. Phys. **47**, 115305 (2014).

[34] R. Monnier and J. P. Perdew, Phys. Rev. B **17**, 2595 (1978).

[35] M. Payne, N. Roberts, R. Needs, M. Needels, and J. Joannopoulos, Surf. Sci. **211–212**, 1 (1989).

[36] X. Leyronas and M. Combescot, Solid State Commun. **119**, 631 (2001).

[37] Y. Tian, M. R. Sakr, J. M. Kinder, D. Liang, M. J. MacDonald, R. L. J. Qiu, H.-J. Gao, and X. P. A. Gao, Nano Lett. **12**, 6492 (2012).

[38] S. Lizzit, K. Pohl, A. Baraldi, G. Comelli, V. Fritzsche, E. Plummer, R. Stumpf, and P. Hofmann, Phys. Rev. Lett. **81**, 3271 (1998).

[39] R. Kammerer, J. Barth, F. Gerken, C. Kunz, S. A. Flodstrøm, and L. I. Johansson, Phys. Rev. B **26**, 3491(R) (1982).